Energy-loss function in the two-pair approximation for the electron liquid

M. E. Bachlechner
Institut für Theoretische Physik, Johannes Kepler Universität, A-4040 Linz, Austria
and Concurrent Computing Laboratory for Materials Simulations, Department of Physics and Astronomy, Department of Computer Science, Louisiana State University, Baton Rouge, Louisiana 70803

A. Holas
Institute of Physical Chemistry, Polish Academy of Sciences, Kasprzaka 44/52, 01-224 Warsaw, Poland

H. M. Böhm
Institut für Theoretische Physik, Johannes Kepler Universität, A-4040 Linz, Austria

A. Schinner
Institut für Experimentalphysik, Abteilung für Atom- und Kernphysik, Johannes Kepler Universität, A-4040 Linz, Austria
(Received 29 December 1995)

The imaginary part of the proper polarizability, Im Π, arising due to excitations of two electron-hole pairs, is studied in detail for electron systems of arbitrary dimensionality, and taking into account arbitrary degeneracy of the electron bands. This allows an application to semiconductors with degenerate valleys, and to ferromagnetic metals. The results obtained not only confirm expressions already known for paramagnetic systems in the high-frequency region, but are also rigorously shown to be valid for all frequencies outside the particle-hole continuum. For a sufficiently high momentum transfer a cutoff frequency (below which Im $\Pi=0$) is established for not only two-pair but also any n-pair processes. In contrast, there is no upper cutoff for $n>1$. The energy-loss function, including the discussed two-pair contributions, is calculated. The effects of screening are investigated. Numerical results, illustrating various aspects and properties of this function, especially showing finite-width plasmon peaks, are obtained for a two-dimensional electron gas.
[S0163-1829(96)00128-2]

I. INTRODUCTION

Dynamic excitations of electronic systems have been widely studied, both by electron-energy-loss spectroscopy (EELS) (Refs. 1–4) and in x-ray scattering experiments.[5–7] The doubly differential scattering cross section measured in these experiments is proportional to the energy-loss function

$$\frac{d^2\sigma}{d\Omega\, d\omega} \propto \mathrm{Im}\left[-\frac{1}{\epsilon(q,\omega)}\right], \tag{1}$$

where q and ω denote the momentum and energy transferred to the system. Whereas in the EELS experiments the long-wavelength region is accessible, measurements using x rays probe the large-q domain. Accordingly, descriptions of the dielectric function $\epsilon(q,\omega)$ which are adequate in the whole (q,ω) plane are required. Measurements for three-dimensional (3D) metals showed that, besides a likely relevance of lattice effects,[5,8] strong many-body correlations beyond the random-phase approximation (RPA) are of crucial importance. In particular, recent x-ray experiments[6] on Al have given strong evidence of the influence of multipair excitations, and many-body effects had to be explicitly invoked to satisfactorily explain the data for Be and Li.[5,9,10]

A number of dynamic theories for the energy-loss function have been reported in the literature, fundamental works being those of Awa, Yasahura, and Asaki,[10] Aravind, Holas, and Singwi,[11] Lee and Hong,[12] Green, Neilson, and Szymanski,[13,14] and Nakano and Ichimaro.[15] The above studies are based on different approaches and ansatzes, but have in common that they globally account for Coulomb correlations to infinite order. It is therefore difficult to use them for estimating the respective contributions of the various possible excitations. However, a better knowledge of the processes involved appears highly desirable for an improved interpretation of the measured spectra. The current work aims at reducing this gap by a detailed investigation of the most prominent multipair process, the excitation of two particle-hole pairs. This information additionally provides valuable input for ion-induced-electron-emission studies.[16,17] As will be demonstrated, the two-pair excitations in the many-electron system represent the leading (lowest perturbation order) virtual processes resulting in a finite width of the plasmon excitations—the most important collective phenomena in the electron liquid, observed at small q as peaks of the energy-loss function (1). Thus our investigation will shed light on these collective excitations, as well as on the dynamic dielectric function [which is involved in Eq. (1)] in metals. The influence of the multipair excitations on the plasmon's dispersion coefficient[18] is beyond the scope of the perturbational approach presented here.

It is convenient to represent the dielectric function ϵ in terms of the proper polarizability Π as

$$\epsilon(q,\omega)=1-v(q)\Pi(q,\omega), \tag{2}$$

with $v(q)$ denoting the Fourier transform of the Coulomb interaction ($4\pi e^2/q^2$ in 3D and $2\pi e^2/q$ in 2D, respectively).

We start by deriving a general property—a lower cutoff frequency of $\mathrm{Im}\,\Pi^{n\mathrm{Pair}}$—due to *arbitrary* n-pair excitations in Sec. II. Subsequently, special emphasis is put on the leading contribution, the excitation of two particle-hole pairs. They are included in the second-order polarizability diagrams (i.e., containing two interaction lines). These diagrams consist of two contributions of different physical origin. Ten of them describe processes where the second electron-hole pair is excited after annihilation of the first pair, so only one electron and one hole exist all the time. The other ten diagrams show two virtual electron-hole pairs propagating simultaneously during some intermediate time interval. These latter diagrams will be the subject of the present analysis.

The first results for the imaginary part of Π due to two-pair excitations, $\mathrm{Im}\,\Pi^{2\mathrm{Pair}}$, have been given by Glick and Long[19] (hereafter referred to as GL) for 3D systems in the high-frequency region. Corresponding studies of the two-dimensional (2D) case were presented by Holas and Singwi.[20] Independent calculations of $\Pi^{2\mathrm{Pair}}$ using either diagrams or Green's functions have resulted in a full complex expression[21–24] involving various products of energy denominators. Besides confirming these results by means of a diagrammatic analysis (Appendix B and Sec. III), the present work explicitly demonstrates in Sec. IV that the validity of the GL formula can be extended for *all* q and for ω both *above* and *below* the single-pair continuum. For the proof, the zeros of all denominators are checked for various ω and q.

A further compelling motivation for studying the two-pair excitations arises from the behavior of modern (quasi-) 2D semiconductor structures [quantum wells and metal-oxide-semiconductor field-effect transistors, (MOSFET's)].[25–27] The plasmon in these systems, experimentally widely studied,[28,29,30] has a lifetime which is substantially influenced by two-pair processes.[31,32] Also, for certain symmetry directions in Si-SiO_2 MOSFET's a valley degeneracy N_{val} of the electron bands occurs in addition to the usual spin degeneracy. Both sources of degeneracy can be combined into an overall degeneracy factor N_d.

$$N_d = N_{\mathrm{spin}} N_{\mathrm{val}}. \tag{3}$$

N_{spin} is 1 in ferromagnetic and 2 in the paramagnetic case. In systems with degenerate valleys, besides $N_{\mathrm{val}}>1$, $N_{\mathrm{val}}=1$ can also be realized, depending on the density.[33,34] Therefore, typical values for N_d are 1,2,4 . . . . For ensuring the correct fulfillment of Pauli's exclusion principle, this degeneracy factor N_d *must* be taken into account. Therefore, the calculation of $\Pi^{2\mathrm{Pair}}$ given in Sec. III is extended to the case of arbitrary degeneracy N_d.

Before using these results for numerical evaluations of the energy-loss function for specific systems, the general investigations are rounded off by a brief study of screening in Sec. V. A standard approach, known in the literature, accounts globally for a class of higher-order processes by replacing the bare interaction, in the (exact) perturbational result, with a screened one.[19,20,35] The application of this procedure to our diagrammatic analysis leads to a split of the final expression into two contributions in which screening may be treated differently and, accordingly, may result in a modification of the GL expression.[19]

All the investigations and results discussed so far hold for both 3D and 2D systems. In the final two sections of this work we apply the developed formalism to the 2D case. In Sec. VI a transformation of variables is presented, allowing for a significantly more efficient numerical evaluation of $\mathrm{Im}\,\Pi^{2\mathrm{Pair}}$. In Sec. VII the energy-loss function is evaluated numerically, and the corresponding data are presented for various densities, momentum transfers, and degeneracies. We conclude with a critical discussion of the applied methods and the obtained results.

II. FREQUENCY RANGE COVERED BY THE n-PAIR CONTRIBUTION TO $\mathrm{Im}\,\Pi(q,\omega)$

Generalizing the known expressions for the one-pair and two-pair cases, the n-(particle-hole)-pair contribution to the imaginary part of the proper polarizability may be written in the form

$$\begin{aligned}\mathrm{Im}\,\Pi^{n\mathrm{Pair}}(q,\omega) = (2\pi)^{-(2n-1)D} \int \left\{ \prod_{j=1}^{n} d^D h_j d^D p_j n^+_{\mathbf{h}_j} n^-_{\mathbf{p}_j} \right\} \\ \times \delta(\mathbf{q}-\mathbf{q}_0)[\,\delta(\omega-\omega_0)-\delta(\omega+\omega_0)\,] \\ \times \mathcal{F}^{n\mathrm{Pair}}(\mathbf{h}_1,\ldots,\mathbf{h}_n,\mathbf{p}_1,\ldots,\mathbf{p}_n),\end{aligned} \tag{4}$$

where

$$\omega_0 \equiv \tfrac{1}{2}[(\mathbf{p}_1^2+\cdots+\mathbf{p}_n^2)-(\mathbf{h}_1^2+\cdots+\mathbf{h}_n^2)] \tag{5}$$

is the n-pair excitation energy, and

$$\mathbf{q}_0 \equiv (\mathbf{p}_1+\cdots+\mathbf{p}_n)-(\mathbf{h}_1+\cdots+\mathbf{h}_n) \tag{6}$$

is the n-pair excitation momentum. The occupation functions

$$n^+_{\mathbf{k}} = \theta(k_F^2-\mathbf{k}^2), \quad n^-_{\mathbf{k}} = \theta(\mathbf{k}^2-k_F^2) \tag{7}$$

in Eq. (4) indicate that the particle momenta are denoted by $\mathbf{p}_j$, the hole ones by $\mathbf{h}_j$ [here $\theta(x)$ is the unit-step function, and k_F the Fermi momentum, and all quantities are measured in atomic units, $\hbar=1=m^*$]. The δ functions impose conservation of the total momentum and energy of the system. Due to the antisymmetry of $\mathrm{Im}\,\Pi(q,\omega)$ with respect to ω, seen in particular in Eq. (4), in the following it is sufficient to consider the $\omega\geqslant 0$ case.

It is known that both the Lindhard function $\Pi_0(q,\omega)$ and the first-order polarizability[36] follow from one-pair excitations only, and, therefore, $\mathrm{Im}\,\Pi^{1\mathrm{Pair}}(q,\omega)$ is zero outside the particle-hole continuum ''strip'' in the $(\mathbf{q},\omega)$ plane. We investigate now if a similar property is connected with any n-(particle-hole)-pairs contribution. Such a strip, if it exists, is defined from below by the minimum value $\omega_{\min}^{n\mathrm{Pair}}(q)$, and from above by the maximum value $\omega_{\max}^{n\mathrm{Pair}}(q)$, of the excitation energy ω_0 at a fixed value of q. The search for these extrema is done in the space of all $\mathbf{h}_j$ and $\mathbf{p}_j$ with the constraints due to their occupation functions and to the momentum conservation, which ties the result to q via $|\mathbf{q}_0|=|\mathbf{q}|=q$. It proves convenient to partition the momentum transfer into separate pair transfers by setting

$$\mathbf{p}_j = \mathbf{h}_j + \alpha_j \mathbf{q}, \tag{8}$$

and then impose the global momentum conservation by the constraint

$$\sum_{j=1}^{n} \alpha_j = 1. \tag{9}$$

Using Eq. (5), this leads to

$$\omega_{\min}^{n\text{Pair}}(q) = \min_{\substack{\alpha_1,\ldots,\alpha_n \\ \alpha_1+\cdots+\alpha_n=1}} \left\{ \sum_{j=1}^{n} \omega_{\min}^{1\text{Pair}}(|\alpha_j|q) \right\}, \tag{10}$$

where

$$\omega_{\min}^{1\text{Pair}}(k) = \min_{\substack{\mathbf{h} \\ \mathbf{h}^2<k_F^2,\ \ |\mathbf{h}+\mathbf{k}|^2>k_F^2}} \tfrac{1}{2}[(\mathbf{h}+\mathbf{k})^2-\mathbf{h}^2]. \tag{11}$$

Analogous relations hold for the upper bound $\omega_{\max}^{n\text{Pair}}(q)$. For $D \geqslant 2$ it is easy to check that the well-known bounds of the $(n=1)$ particle-hole continuum are obtained as

$$\omega_{\max}^{1\text{Pair}}(k) = \omega_{1P+}(k), \tag{12}$$

$$\omega_{\min}^{1\text{Pair}}(k) = \omega_{1P-}(k)\,\theta(\omega_{1P-}(k)), \tag{13}$$

with

$$\omega_{1P\pm}(k) = \tfrac{1}{2}k(k \pm 2k_F). \tag{14}$$

In order to estimate $\omega_{\max}^{n\text{Pair}}(q)$ for $n \geqslant 2$ from the ''maximum'' analog of Eq. (10), the n-dimensional trial vector $\boldsymbol{\alpha}=(\alpha_1,1-\alpha_1,0,\ldots,0)$ is considered. This obviously satisfies the constraint (9) and leads to the inequality

$$\omega_{\max}^{n\text{Pair}} \geqslant \omega_{\max}^{1\text{Pair}}(|\alpha_1|q) + \omega_{\max}^{1\text{Pair}}(|\alpha_1-1|q). \tag{15}$$

In the limit $|\alpha_1| \to \infty$, both terms on the right-hand side of Eq. (15) tend to infinity, so that, in contrast to the single-pair excitations, the multipair contributions are not bound from above, i.e.,

$$\omega_{\max}^{n\text{Pair}}(q) = +\infty \quad \text{for } n \geqslant 2. \tag{16}$$

The lower bound, however, is found to be finite for all n-pair excitations. Leaving details of the derivation to Appendix A, this bound is obtained as

$$\omega_{\min}^{n\text{Pair}}(q) = \omega_{nP-}(q)\,\omega(\omega_{nP-}(q)), \tag{17}$$

with

$$\omega_{nP\pm}(k) = \frac{1}{2n}\,k(k \pm 2nk_F) \tag{18}$$

being a generalization of the single-pair case (14).

Thus, whereas single-pair excitations make a nonzero contribution to $\mathrm{Im}\,\Pi(q,\omega)$ in a strip $\omega_{\min}^{1\text{Pair}} < \omega < \omega_{\max}^{1\text{Pair}}(q)$—the particle-hole continuum range, multipair excitations make such a contribution in a semi-infinite frequency range $\omega > \omega_{\min}^{n\text{Pair}}(q)$.

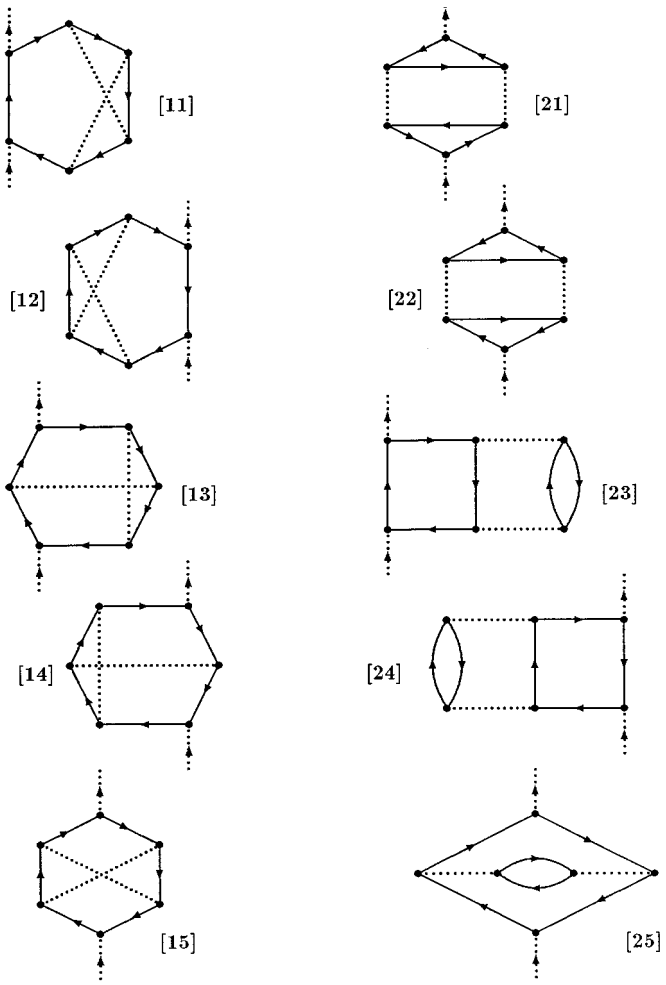

FIG. 1. The ten second-order polarization diagrams describing ''true'' two-pair processes. The lines with arrows denote the free single-particle propagators, the dotted lines are the bare Coulomb interactions. Dotted lines with arrows show the vertices of entrance/exit for each diagram.

III. TWO-PAIR CONTRIBUTION TO Im $\Pi(q,\omega)$ IN THE SECOND-ORDER APPROXIMATION

The ten second-order Feynman diagrams containing ''true'' two-pair excitations are displayed in Fig. 1. (Here we also note a misprint in Fig. 2 of GL: diagrams *i* and *h* are equivalent, whereas the analog to *f*, but with opposite arrow directions, is missing.) The resulting complex $\Pi(q,\omega)$ obtained by evaluating and summing these ten diagrams (cf. Appendix B) contains both single- and two-pair contributions. For the imaginary part of Π the latter are separated out in the form

$$\begin{aligned} \mathrm{Im}\,\Pi^{2\,\text{Pair}}(q,\omega;[v]) = \Omega_D^{-3} \sum_{\mathbf{q}_1,\mathbf{q}_2,\mathbf{q}_3,\mathbf{q}_4} & n_{\mathbf{q}_1}^{+} n_{\mathbf{q}_2}^{+} n_{\mathbf{q}_3}^{-} n_{\mathbf{q}_4}^{-} \\ & \times \delta_{\mathbf{q},\mathbf{q}_3+\mathbf{q}_4-\mathbf{q}_1-\mathbf{q}_2} \\ & \times [\,\delta(\omega-\omega_0) - \delta(\omega+\omega_0)\,] \\ & \times \mathcal{F}^{2\,\text{Pair}}(\mathbf{q}_1,\ldots,\mathbf{q}_4,N_d;[v]), \end{aligned} \tag{19}$$

where Ω_D is the D-dimensional volume of the system, and

$$\mathcal{F}^{2\,\mathrm{Pair}}=N_d^2\left\{\sum_{j=1}^{5}\mathcal{F}_{[2j]}(\mathbf{q}_1,\ldots,\mathbf{q}_4;[v])\right\}-N_d\left\{\sum_{j=1}^{5}\mathcal{F}_{[1j]}(\mathbf{q}_1,\ldots,\mathbf{q}_4;[v])\right\}. \tag{20}$$

Here $\mathcal{F}_{[1j]}$ represents the contribution of the one-fermion-loop diagram $1j$, and $\mathcal{F}_{[2j]}$ the same for the two-loop diagram $2j$. In Eq. (20) the dependence on the total degeneracy N_d of the electron conduction band [cf. Eq. (3)] is seen explicitly. It is obtained via an extension of the usual summation over two spin states to N_d states, performed separately for each fermion loop. Besides N_d, a factor (-1) is also connected with each loop. The two-pair excitation energy [compare Eq. (5)] is

$$\omega_0=\omega_0(\mathbf{q}_1,\ldots,\mathbf{q}_4)=\epsilon_3+\epsilon_4-\epsilon_1-\epsilon_2\geqslant 0, \tag{21}$$

where

$$\epsilon_i\equiv\epsilon_{\mathbf{q}_i}\equiv\tfrac{1}{2}\mathbf{q}_i^2 \tag{22}$$

is the free-electron energy. The occupation factors $n_{\mathbf{k}}^{\pm}$ are defined in Eq. (7).

The evaluation of the diagrams in Appendix B results in

$$\pi^{-1}\sum_{j=1}^{5}\mathcal{F}_{[1j]}=2(v_{31}v_{32}+v_{31}v_{41})\omega_{2'}^{-1}\omega_{4'}^{-1}-v_{41}v_{31}(\omega_{2'}^{-2}+\omega_{3'}^{-1}\omega_{4'}^{-1})-v_{41}v_{42}(\omega_{3'}^{-2}+\omega_{1'}^{-1}\omega_{2'}^{-1}), \tag{23}$$

$$\pi^{-1}\sum_{j=1}^{5}\mathcal{F}_{[2j]}=2(v_{41}v_{32}+v_{31}^2)\omega_{2'}^{-1}\omega_{4'}^{-1}-v_{41}^2(\omega_{2'}^{-2}+\omega_{3'}^{-2})-v_{41}v_{32}(\omega_{1'}^{-1}\omega_{2'}^{-1}+\omega_{3'}^{-1}\omega_{4'}^{-1}). \tag{24}$$

Herein the abbreviations $\omega_{i'}$ denote the occurring combinations of energies, namely

$$\begin{aligned}\omega_{1'}&=\epsilon_3+\epsilon_4-\epsilon_{1'}-\epsilon_2=(\mathbf{q}_3-\mathbf{q}_2)\cdot(\mathbf{q}_4-\mathbf{q}_2),\\ \omega_{2'}&=\epsilon_3+\epsilon_4-\epsilon_1-\epsilon_{2'}=-(\mathbf{q}_3-\mathbf{q}_1)\cdot(\mathbf{q}_4-\mathbf{q}_1),\\ \omega_{3'}&=\epsilon_{3'}+\epsilon_4-\epsilon_1-\epsilon_2=+(\mathbf{q}_4-\mathbf{q}_1)\cdot(\mathbf{q}_4-\mathbf{q}_2),\\ \omega_{4'}&=\epsilon_3+\epsilon_{4'}-\epsilon_1-\epsilon_2=+(\mathbf{q}_3-\mathbf{q}_1)\cdot(\mathbf{q}_3-\mathbf{q}_2),\end{aligned} \tag{25}$$

with the corresponding momenta

$$\begin{aligned}\mathbf{q}_{1'}&=\mathbf{q}_3+\mathbf{q}_4-\mathbf{q}_2=\mathbf{q}_1+\mathbf{q},\\ \mathbf{q}_{2'}&=\mathbf{q}_3+\mathbf{q}_4-\mathbf{q}_1=\mathbf{q}_2+\mathbf{q},\\ \mathbf{q}_{3'}&=\mathbf{q}_1+\mathbf{q}_2-\mathbf{q}_4=\mathbf{q}_3-\mathbf{q},\\ \mathbf{q}_{4'}&=\mathbf{q}_1+\mathbf{q}_2-\mathbf{q}_3=\mathbf{q}_4-\mathbf{q}.\end{aligned} \tag{26}$$

The potential factors v_{ij} are defined as

$$v_{ij}=v(\mathbf{q}_i-\mathbf{q}_j). \tag{27}$$

The above equations (23) and (24) are valid under the assumption that $\omega_{i'}\neq 0$ during integrations over $\mathbf{q}_i$.

Because all elements of Eq. (19) except $\mathcal{F}^{2\,\mathrm{Pair}}$ are symmetrical with respect to $\mathbf{q}_1\leftrightarrow\mathbf{q}_2$ and $\mathbf{q}_3\leftrightarrow\mathbf{q}_4$, the value of $\mathrm{Im}\,\Pi^{2\,\mathrm{Pair}}$ remains unchanged after such a symmetrization of expressions (23) and (24),

$$\pi^{-1}\sum_{j=1}^{5}\mathcal{F}_{[1j]}=(-\tfrac{1}{2})[v_{31}(\omega_{4'}^{-1}-\omega_{2'}^{-1})+v_{42}(\omega_{3'}^{-1}-\omega_{1'}^{-1})]\times[v_{32}(\omega_{4'}^{-1}-\omega_{1'}^{-1})+v_{41}(\omega_{3'}^{-1}-\omega_{2'}^{-1})], \tag{28}$$

$$\pi^{-1}\sum_{j=1}^{5}\mathcal{F}_{[2j]}=(-\tfrac{1}{4})\{[v_{31}(\omega_{4'}^{-1}-\omega_{2'}^{-1})+v_{42}(\omega_{3'}^{-1}-\omega_{1'}^{-1})]^2+[v_{32}(\omega_{4'}^{-1}-\omega_{1'}^{-1})+v_{41}(\omega_{3'}^{-1}-\omega_{2'}^{-1})]^2\}. \tag{29}$$

After inserting expressions (28) and (29) into Eq. (20), the final result is obtained with the integrand negative everywhere:

$$\mathcal{F}^{2\,\mathrm{Pair}}(\mathbf{q}_1,\ldots,\mathbf{q}_4,N_d;[v])=-\frac{\pi}{4}N_d\{(N_d-1)[(A_{31}+A_{42})^2+(A_{32}+A_{41})^2]+[(A_{31}+A_{42})+(A_{32}+A_{41})]^2\}, \tag{30}$$

where

$$A_{ph}(\mathbf{q}_1,\ldots,\mathbf{q}_4;[v])=v(\mathbf{q}_p-\mathbf{q}_h)\,\frac{(\mathbf{q}_p-\mathbf{q}_h)\cdot(\mathbf{q}_p+\mathbf{q}_{\dot p}-\mathbf{q}_h-\mathbf{q}_{\dot h})}{[(\mathbf{q}_p-\mathbf{q}_h)\cdot(\mathbf{q}_p-\mathbf{q}_{\dot h})][(\mathbf{q}_p-\mathbf{q}_h)\cdot(\mathbf{q}_{\dot p}-\mathbf{q}_h)]}. \tag{31}$$

The pairs of indices occurring therein are

$$(h,\dot h)=(1,2)\ \text{ or }\ (2,1);\quad (p,\dot p)=(3,4)\ \text{ or }\ (4,3), \tag{32}$$

so in any case $\mathbf{q}_p+\mathbf{q}_{\dot p}-\mathbf{q}_h-\mathbf{q}_{\dot h}=\mathbf{q}$ holds due to the momentum-conservation δ function in Eq. (19).

For $N_d=2$ (spin degeneracy only) the obtained result is

equivalent to the symmetrized GL result,[19] valid, according to their claim, in the high-frequency region. In Sec. IV we determine the range of validity more precisely.

IV. FREQUENCY RANGE FOR WHICH THE ASSUMPTION OF NONZERO DENOMINATORS IS SATISFIED

We claim that the conditions $\omega_{i'} \neq 0$, $i=1$, 2, 3, and 4, allowing the use in Eq. (19) of the integrand $\mathcal{F}^{2\,\mathrm{Pair}}$ in the form (30), are fulfilled for ω lying outside the particle-hole continuum. For the proof we assume that $\omega_{i'}=0$, from which the contradiction is obtained, that some $\mathbf{q}_j$ is outside the integration range defined by $n^{\pm}_{\mathbf{q}_j}$. Again, because of the antisymmetry of $\mathrm{Im}\,\Pi(q,\omega)$, it is sufficient to consider $\omega \geqslant 0$. From now on, we introduce system units: the Fermi momentum k_F for momenta, and the double Fermi energy $2E_F = k_F^2$ for energies.

We start with the case $i=1$ and use relations (25) and (26) to obtain

$$\begin{aligned} 0 = \omega_{1'} &= (\epsilon_3 + \epsilon_4 - \epsilon_1 - \epsilon_2) - (\epsilon_{1'} - \epsilon_1) \\ &= \omega_0 - \tfrac{1}{2}[(\mathbf{q}_1 + \mathbf{q})^2 - \mathbf{q}_1^2]. \end{aligned} \tag{33}$$

For $\omega > 0$ we have $\omega_0 = \omega$ due to the δ function in Eq. (19), so from Eq. (33) it follows that $\mathbf{q}_1 \cdot (\mathbf{q}/q) = \omega/q - q/2$, and we end up with

$$\mathbf{q}_1^2 \geqslant C(q,\omega), \tag{34}$$

where

$$C(q,\omega) = \left(\frac{\omega}{q} - \frac{q}{2}\right)^2. \tag{35}$$

In the frequency range *above* the particle-hole continuum, $\omega > \omega_{1P+}(q) = \frac{1}{2}q^2 + q$ [cf. Eq. (12)], from Eq. (35) we have

$$C(q,\omega) = \left[\left(\frac{\omega - \omega_{1P+}(q)}{q} + \frac{q}{2} + 1\right) - \frac{q}{2}\right]^2 > 1, \tag{36}$$

whereas *below* the continuum, $0 < \omega < \omega_{1P-}(q) = \frac{1}{2}q^2 - q$ for $q > 2$, [cf. Eq. (13)], we get

$$C(q,\omega) = \left[\left(-\frac{\omega_{1P-}(q) - \omega}{q} + \frac{q}{2} - 1\right) - \frac{q}{2}\right]^2 > 1. \tag{37}$$

Both Eqs. (36) and (37) show that $\mathbf{q}_1$ in Eq. (34) is outside the integration range limited by $n^{+}_{\mathbf{q}_1}$ in Eq. (19). Due to the symmetry with respect to the holes, this proof also holds for $i=2$.

Next the case $i=3$ is considered. As before,

$$\begin{aligned} 0 = \omega_{3'} &= (\epsilon_3 + \epsilon_4 - \epsilon_1 - \epsilon_2) - (\epsilon_3 - \epsilon_{3'}) \\ &= \omega_0 + \tfrac{1}{2}[(\mathbf{q}_3 - \mathbf{q})^2 - \mathbf{q}_3^2]. \end{aligned} \tag{38}$$

So at $\omega_0 = \omega$, we obtain $(\mathbf{q}_3 - \mathbf{q}) \cdot \mathbf{q}/q = \omega/q - q/2$, which results in

$$(\mathbf{q}_3 - \mathbf{q})^2 \geqslant C(q,\omega). \tag{39}$$

Using an alternative representation for ω_3 from Eq. (25), we have

$$\begin{aligned} 0 = \omega_{3'} &= (\mathbf{q}_4 - \mathbf{q}_1) \cdot (\mathbf{q}_4 - \mathbf{q}_2) \\ &= (\mathbf{q}_2 + \mathbf{q} - \mathbf{q}_3) \cdot (\mathbf{q}_1 + \mathbf{q} - \mathbf{q}_3) \\ &= \mathbf{q}_1 \cdot \mathbf{q}_2 + (\mathbf{q}_1 + \mathbf{q}_2) \cdot (\mathbf{q} - \mathbf{q}_3) + (\mathbf{q} - \mathbf{q}_3)^2. \end{aligned} \tag{40}$$

With the help of Eq. (40), the value of $\mathbf{q}_4^2$ can be obtained in the form

$$\mathbf{q}_4^2 = (\mathbf{q}_1 + \mathbf{q}_2 + \mathbf{q} - \mathbf{q}_3)^2 = \mathbf{q}_1^2 + \mathbf{q}_2^2 + (1-2)(\mathbf{q} - \mathbf{q}_3)^2. \tag{41}$$

Taking into account Eq. (39) and the inequalities $\mathbf{q}_1^2 \leqslant 1$ and $\mathbf{q}_2^2 \leqslant 1$, we estimate $\mathbf{q}_4^2$ as

$$\mathbf{q}_4^2 \leqslant 2 - C(q,\omega). \tag{42}$$

However, for ω lying outside the particle-hole continuum, we have $C(q,\omega) > 1$; see Eqs. (36) and (37). Therefore Eq. (42) leads to

$$\mathbf{q}_4^2 < 1, \tag{43}$$

i.e., $\mathbf{q}_4$ is outside the integration range limited by $n^{-}_{\mathbf{q}_4}$ in Eq. (19). Again, the proof can be extended to $i=4$ by symmetry considerations.

V. MODIFICATION OF $\mathrm{Im}\,\Pi(q,\omega)$ BY MEANS OF SCREENING OF THE ELECTRON-ELECTRON INTERACTION

As was noticed by previous workers,[19,20,23,35,37] when the second-order expression for $\mathrm{Im}\,\Pi^{2\,\mathrm{Pair}}$, Eqs. (19) and (30), is used for the calculation of the plasmon damping, the obtained results show a strong overdamping in comparison with the experimental data. This means that the nth order in v contributions to $\mathrm{Im}\,\Pi(q,\omega)$, $n > 2$, are important. One idea to include some infinite class of higher-order diagrams is to replace the bare electron-electron interaction lines in the ten second-order diagrams of Fig. 1 by ''dressed'' lines (representing the screened interaction). In order to avoid double counting of some diagrams, such a replacement can be applied to the ''skeleton'' diagrams only.[38] Among the diagrams in Fig. 1, these denoted by ''23,'' ''24,'' and ''25'' do not belong to this class. They may be viewed as first-order diagrams modified in such a way that their bare interaction line is replaced by the line with one loop (the zeroth-order polarizability Π_0) inserted into it. Such a modification represents only one of an infinite number of terms which sum up to form the RPA screened interaction

$$\tilde{v}(\mathbf{p},p_0) = \frac{v(\mathbf{p})}{1 - v(\mathbf{p})\Pi_0(\mathbf{p},p_0)} = \frac{v(\mathbf{p})}{\epsilon^{\mathrm{RPA}}(\mathbf{p},p_0)} \tag{44}$$

[here the argument pair $(\mathbf{p},p_0)$ represents momentum and frequency components of the $(D+1)$-dimensional argument vector, as it is adopted in Appendix B]. Therefore, the correct way to include screening in the mentioned diagrams is to

replace the term which represents the two interaction lines with a bubble between them (see, e.g., Fig. 7) with the following expression:

$$\tilde{\hat{V}}(\mathbf{p},p_0)\Pi_0(\mathbf{p},p_0)=\tilde{v}(\mathbf{p},p_0)-v(\mathbf{p})=\frac{[v(\mathbf{p})]^2\Pi_0(\mathbf{p},p_0)]}{1-v(\mathbf{p})\Pi_0(\mathbf{p},p_0)}. \tag{45}$$

The leading term of a formal expansion of expression (45) in powers of v,

$$\tilde{\hat{V}}(\mathbf{p},p_0)\Pi_0(\mathbf{p},p_0)=[v(\mathbf{p})]^2\Pi_0(\mathbf{p},p_0)+O(v^3), \tag{46}$$

represents the original contribution (before screening), which demonstrates the correctness of the proposed replacement.

In order to evaluate the expressions for $\mathrm{Im}\,\Pi^{2\,\mathrm{Pair}}$ efficiently, we need to introduce an additional approximation that neglects the frequency dependence of $\epsilon^{\mathrm{RPA}}(\mathbf{p},p_0)$. Following the arguments given by GL[19] static screening is chosen in all diagrams contributing to the imaginary part of the dielectric function. In contrast to GL, however, where the Thomas-Fermi interaction was used, we take the static RPA dielectric function $\epsilon^{\mathrm{RPA}}(\mathbf{p},0)$ to screen the potential in a way which is valid also for a larger momentum range. Therefore, we finally obtain

$$\tilde{\hat{V}}(\mathbf{p},p_0)\Pi_0(\mathbf{p},p_0)\approx\tilde{\hat{V}}(\mathbf{p})\Pi_0(\mathbf{p},p_0), \tag{47}$$

where the replacement due to screening is [see Eq. (45)]

$$\hat{V}(\mathbf{p})\rightarrow\tilde{\hat{V}}(\mathbf{p})=\frac{v^2(\mathbf{p})}{\epsilon^{\mathrm{RPA}}(\mathbf{p},0)}=\tilde{v}^2(\mathbf{p})[1-v(\mathbf{p})\Pi_0(\mathbf{p},0)], \tag{48}$$

with [see Eq. (44)]

$$\tilde{v}(\mathbf{p})\equiv\tilde{v}(\mathbf{p},0)=\frac{v(\mathbf{p})}{\epsilon^{\mathrm{RPA}}(\mathbf{p},0)}. \tag{49}$$

Accordingly, for the evaluation of $\mathrm{Im}\,\Pi^{2\,\mathrm{Pair}}$ with the screened interaction, this potential $\tilde{\hat{V}}(\mathbf{p})$ should replace $\hat{V}_{[a]}$ for $a=24$, 23, and 25 in Eq. (92), etc. For the remaining diagrams, $\hat{V}_{[a]}$ should be modified in Eq. (B16), etc. according to

$$v(\mathbf{p})v(\mathbf{k})\rightarrow\tilde{v}(\mathbf{p})\tilde{v}(\mathbf{k}). \tag{50}$$

In the above equations $\epsilon^{\mathrm{RPA}}(p,0)$ can be replaced by another chosen model static dielectric function $\epsilon^{M}(p)$.

At this point we note that the result obtained in this way differs from previous calculations (e.g., Refs. 32, 19, 20, and 35), where the replacement (50) was used for *all* v factors in the second-order expression. In the further discussion such results will be called *overall screened* (OS). As the most refined version of such approaches[32] has led to very satisfactory results both in comparison with other theories[39] and experiment,[4] it is not *a priori* obvious that this procedure gives results inferior to those obtained with Eq. (48) for the terms discussed above. These will be referred to as *selectively screened* (SS) in the following. We now derive the corresponding expressions for $\mathcal{F}^{2\,\mathrm{Pair}}$, while the results will be discussed in Sec. VII.

After inserting the replacements (48) and (50) into Eqs. (23) and (24), we obtain the following expression for $\mathcal{F}^{2\,\mathrm{Pair}}_{\mathrm{SS}}$, which replaces $\mathcal{F}^{2\,\mathrm{Pair}}$ in Eq. (19) when selective screening is included,

$$\mathcal{F}^{2\,\mathrm{Pair}}_{\mathrm{SS}}(\mathbf{q}_1,\ldots,\mathbf{q}_4,N_d;[v])=\mathcal{F}^{2\,\mathrm{Pair}}(\mathbf{q}_1,\ldots,\mathbf{q}_4,N_d;[\tilde{v}])+\mathcal{F}^{2\,\mathrm{Pair}}_{\mathrm{DIF}}(\mathbf{q}_1,\ldots,\mathbf{q}_4,N_d;[\tilde{v}]). \tag{51}$$

The first term represents the standard overall-screened contribution, and the second one the difference (DIF) between the two approaches in the following form

$$\mathcal{F}^{2\,\mathrm{Pair}}_{\mathrm{DIF}}(\mathbf{q}_1,\ldots,\mathbf{q}_4,N_d;[\tilde{v}])=-\frac{\pi}{4}N_d^2[Q_{31}\tilde{A}^2_{31}+Q_{42}\tilde{A}^2_{42}+Q_{32}\tilde{A}^2_{32}+Q_{41}\tilde{A}^2_{41}], \tag{52}$$

where

$$Q_{\mathrm{ph}}=Q^{\mathrm{RPA}}(|\mathbf{q}_p-\mathbf{q}_h|,0)\equiv\epsilon^{\mathrm{RPA}}(\mathbf{q}_p-\mathbf{q}_h,0)-1>0 \tag{53}$$

and

$$\tilde{A}_{\mathrm{ph}}=A_{\mathrm{ph}}(\ldots;[\tilde{v}]), \tag{54}$$

see Eq. (31). Expression (52) for $\mathcal{F}^{2\mathrm{Pair}}_{\mathrm{DIF}}$ follows from the second term in the square brackets in Eq. (48), applied to these elements of Eq. (30) which belong to two-fermion-loop diagrams ($\propto N_d^2$) and contain a squared potential. As the static Lindhard function Π_0 is negative and the bare potential is positive, $Q^{\mathrm{RPA}}(k,0)$ is positive for any k [cf. Eq. (53)]. Therefore, the two terms in Eq. (51) are of the same sign: the DIF part enhances the overall-screened one.

VI. TRANSFORMATION OF VARIABLES FOR AN EFFICIENT NUMERICAL EVALUATION OF $\mathrm{Im}\,\Pi^{2\mathrm{Pair}}$ IN 2D

In the thermodynamic limit, where summations over momenta are replaced by integrations, and again using the system units of k_F and $2E_F$ for momenta and energies, Eq. (19) takes the form

$$\mathrm{Im}\Pi^{2\mathrm{Pair}}(q,\omega)=(2\pi)^{-3D}[I(q,\omega)-I(q,-\omega)], \tag{55}$$

where

$$I(q,\omega)=\int d^Dq_1d^Dq_2d^Dq_3d^Dq_4\,\theta(1-q_1^2)\,\theta(1-q_2^2)\times\theta(q_3^2-1)\,\theta(q_4^2-1)\,\delta[(\mathbf{q}_3+\mathbf{q}_4)-(\mathbf{q}_1+\mathbf{q}_2+\mathbf{q})]\times\delta\left(\frac{(q_3^2+q_4^2)-(q_1^2+q_2^2)}{2}-\omega\right)\times\mathcal{F}(\mathbf{q}_1,\mathbf{q}_2,\mathbf{q}_3,\mathbf{q}_4). \tag{56}$$

For $D=2$ the potential in the system units is $v(q)=2\pi\alpha_2(N_d)r_s/q$, where $\alpha_2(N_d)=(N_d/4)^{1/2}$, and r_s is the density parameter connected with the area density n_2 via $r_sa_B^*=(\pi n_2)^{-1/2}$, while for $D=3$ we have $v(q)=4\pi\alpha_3(N_d)r_s/q^2$, with $\alpha_3(N_d)=(2N_d/(9\pi))^{1/3}$ and $r_sa_B^*=(\frac{4}{3}\pi n_3)^{-3}$. Using the above notations, $k_Fa_B^*$

TABLE I. The auxiliary variables μ_0, μ, α, a_0, ϕ_{10}, ϕ_{20}, and ϕ_{40}, and the vectors $\mathbf{k}_1,\ldots,\mathbf{k}_4$ defined in terms of q, ω, $\zeta_1,\ldots,\zeta_5$ for the integral Eq. (67). * is the equation to obtain $\hat{\phi}_3$ in the range $0\leqslant\phi_3<2\pi$.

1.	$\mu_0=\max(0,1-\omega)$	12.	$\mathbf{k}_1=k_1\mathbf{n}(\phi_1)$
2.	$\mu=\mu_0+(1-\mu_0)\zeta_1$	13.	$\mathbf{k}_2=k_2\mathbf{n}[\phi_1+\phi_{20}+(\pi-2\phi_{20})\zeta_4]$
3.	$\alpha=\pi/2\ \zeta_2$	14.	$\mathbf{k}_3=(k_{3x},k_{3y})=q\mathbf{n}(0)+\mathbf{k}_1$
4.	$k_1=2\mu^{1/2}\cos(\alpha)$	15.	$k_3=(k_{3x}^2+k_{3y}^2)^{1/2}$
5.	$k_2=\mu^{1/2}\sin(\alpha)$	*16.	$\mathbf{n}(\phi_3)=\mathbf{k}_3/k_3$
6.	$a_0=\omega-\frac{1}{4}q^2+k_2^2+\frac{1}{2}k_1q$	17.	$a_4=\omega-\frac{1}{4}q^2+k_2^2-\frac{1}{2}\mathbf{k}_1\cdot\mathbf{q}$
7.	$a_1=(\omega-\frac{1}{4}q^2+k_2^2)/(\frac{1}{2}k_1q)$	18.	$k_4=a_4^{1/2}$
8.	$\phi_{10}=\arccos(\min(1,a_1))$	19.	$a_3=(\mu+\omega-1)/(k_3k_4)$
9.	$a_2=(1-\mu)/(k_1k_2)$	20.	$\phi_{40}=\arccos(\min(1,a_3))$
10.	$\phi_{20}=\arccos(\min(1,a_2))$	21.	$\mathbf{k}_4=k_4\mathbf{n}[\phi_3+\phi_{40}+(\pi-2\phi_{40})\zeta_5]$
11.	$\phi_1=\phi_{10}+2(\pi-\phi_{10})\zeta_3$		

$=[\alpha_D(N_d)r_s]^{-1}$ in D dimensions. As discussed previously, $\mathcal{F}=\mathcal{F}^{\mathrm{2Pair}}$, given by Eqs. (30)–(32), shows the symmetry

$$\mathcal{F}(\mathbf{q}_1,\mathbf{q}_2,\mathbf{q}_3,\mathbf{q}_4)=\mathcal{F}(\mathbf{q}_2,\mathbf{q}_1,\mathbf{q}_3,\mathbf{q}_4)=\mathcal{F}(\mathbf{q}_1,\mathbf{q}_2,\mathbf{q}_4,\mathbf{q}_3). \tag{57}$$

The presence of the δ functions allows us to reduce the dimensionality of the integration by $(D+1)$, but the integration hypervolume in the remaining $(3D-1)$-dimensional space has such a complicated shape that a Monte Carlo method must be used. The fact that the integrand has a definite sign (when ω is outside the particle-hole continuum) is very helpful in obtaining accurate results with this method.

For $D=2$ a transformation of variables, reducing this five-dimensional volume to a hypercube with a unit edge, is shown below. As a first step additional vector variables of integration $\mathbf{k}_1$, $\mathbf{k}_2$, $\mathbf{k}_3$, and $\mathbf{k}_4$ are introduced via

$$\begin{aligned}\mathbf{k}_1&=\mathbf{q}_2+\mathbf{q}_1 & \mathbf{q}_1&=\mathbf{k}_1/2-\mathbf{k}_2\\ &\Leftrightarrow & &\\ \mathbf{k}_2&=(\mathbf{q}_2-\mathbf{q}_1)/2 & \mathbf{q}_2&=\mathbf{k}_1/2+\mathbf{k}_2,\end{aligned} \tag{58}$$

$$\begin{aligned}\mathbf{k}_3&=\mathbf{q}_4+\mathbf{q}_3 & \mathbf{q}_3&=\mathbf{k}_3/2-\mathbf{k}_4\\ &\Leftrightarrow & &\\ \mathbf{k}_4&=(\mathbf{q}_4-\mathbf{q}_3)/2 & \mathbf{q}_4&=\mathbf{k}_3/2+\mathbf{k}_4.\end{aligned} \tag{59}$$

The Jacobian of this transformation is 1. The function $\mathcal{F}^{\mathcal{T}}$, obtained from $\mathcal{F}$ by means of transformations (58) and (59),

$$\mathcal{F}^{\mathcal{T}}(\mathbf{k}_1,\mathbf{k}_2,\mathbf{k}_3,\mathbf{k}_4)=\mathcal{F}\left(\frac{\mathbf{k}_1}{2}-\mathbf{k}_2,\ldots,\frac{\mathbf{k}_3}{2}+\mathbf{k}_4\right), \tag{60}$$

has the property

$$\begin{aligned}\mathcal{F}^{\mathcal{T}}(\mathbf{k}_1,\mathbf{k}_2,\mathbf{k}_3,\mathbf{k}_4)&=\mathcal{F}^{\mathcal{T}}(\mathbf{k}_1,-\mathbf{k}_2,\mathbf{k}_3,\mathbf{k}_4)\\&=\mathcal{F}^{\mathcal{T}}(\mathbf{k}_1,\mathbf{k}_2,\mathbf{k}_3,-\mathbf{k}_4)\end{aligned} \tag{61}$$

due to the symmetry of $\mathcal{F}$, Eq. (57). Therefore, the angular integration over $\mathbf{k}_2$ and $\mathbf{k}_4$ can be performed in a half space only with a doubled integrand. In terms of a unit vector function

$$\mathbf{n}(\phi)=(\cos(\phi),\sin(\phi)) \tag{62}$$

in the coordinate system connected with the vector $\mathbf{q}=q\mathbf{n}(0)=(q,0)$, we define angular variables of integration ϕ_1, ϕ_2, ϕ_3, and ϕ_4 via the relations

$$\mathbf{k}_1=k_1\mathbf{n}(\phi_1),\quad \mathbf{k}_2=k_2\mathbf{n}(\phi_1+\phi_2), \tag{63}$$

$$\mathbf{k}_3=k_3\mathbf{n}(\phi_3),\quad \mathbf{k}_4=k_4\mathbf{n}(\phi_3+\phi_4), \tag{64}$$

so we have $\mathbf{k}_1\cdot\mathbf{k}_2=k_1k_2\cos(\phi_2)$ and $\mathbf{k}_3\cdot\mathbf{k}_4=k_3k_4\cos(\phi_4)$. The momentum- and energy-conservation δ functions rewritten in our new variables are

$$\delta[\mathbf{k}_3-(\mathbf{q}+\mathbf{k}_1)]\,\delta\left[k_4^2-\left(\frac{k_1^2-k_3^2}{4}+k_2^2+\omega\right)\right]. \tag{65}$$

After integration in the whole $\mathbf{k}_3$ space and over the radius k_4 in the $\mathbf{k}_4$ space, we obtain

$$\begin{aligned}I(q,\omega)=&\int d^2k_1d^2k_2\,\theta(1-q_1^2)\,\theta(1-q_2^2)\,\theta(a_4)\\&\times\int_0^{\pi}d\phi_4\,\theta(q_3^2-1)\,\theta(q_4^2-1)\,\mathcal{F}^{\mathcal{T}}(\mathbf{k}_1,\mathbf{k}_2,\mathbf{k}_3,\mathbf{k}_4),\end{aligned} \tag{66}$$

where $\mathbf{k}_3=\mathbf{q}+\mathbf{k}_1$, $a_4=\omega-\frac{1}{4}q^2-\frac{1}{2}\mathbf{q}\cdot\mathbf{k}_1+k_2^2$, and $\mathbf{k}_4=a_4^{1/2}\mathbf{n}(\phi_3+\phi_4)$. In the next step, the occupation factors concerning $\mathbf{q}_3$ and $\mathbf{q}_4$ are exploited to determine the actual integration limits for ϕ_4, and this integral is then transformed to a unit-interval one over ζ_5. Similarly, integrations over ϕ_2 and ϕ_1 are transformed to those over ζ_4 and ζ_3. In the final step a two-dimensional vector $(\frac{1}{2}k_2,k_1)$ is represented in polar coordinates as $\mu^{1/2}[\cos(\alpha),\sin(\alpha)]$ and then variables μ and α are transformed to unit intervals in terms of ζ_1 and ζ_2. Finally we obtain

$$\begin{aligned}I(q,\omega)=&2\pi\theta(\omega)(1-\mu_0)\int_0^1d\zeta_1\mu\int_0^1d\zeta_2\sin(2\alpha)\,\theta(a_0)\\&\times(\pi-\phi_{10})(\pi-2\phi_{20})\int_0^1d\zeta_3\int_0^1d\zeta_4\\&\times(\pi-2\phi_{40})\int_0^1d\zeta_5\mathcal{F}^{\mathcal{T}}(\mathbf{k}_1,\mathbf{k}_2,\mathbf{k}_3,\mathbf{k}_4),\end{aligned} \tag{67}$$

where the auxiliary variables μ_0, μ, α, a_0, ϕ_{10}, ϕ_{20}, and ϕ_{40} and the vectors $k_1,\ldots,k_4$ defined in terms of q, ω,

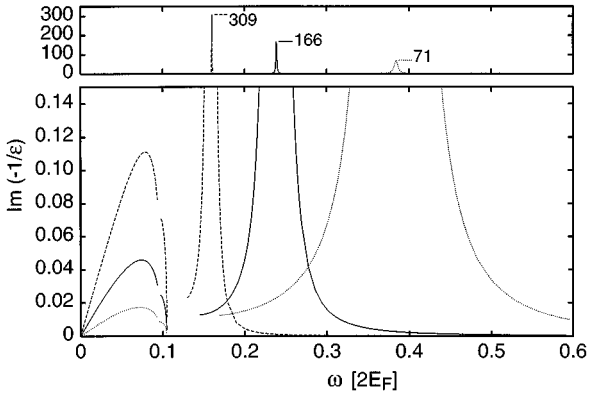

FIG. 2. Energy-loss function of an electron layer at $r_s=0.7$, calculated with the unscreened interaction. The momentum transfer q of all three curves was taken to be $0.1k_F$. Dashed line: $N_d=1$; full line: $N_d=2$ (i.e., the most commonly realized case of nondegenerate valleys and two spin possibilities); dotted line: $N_d=4$. Upper part: the full ordinate is shown in order to display the relative heights of the peaks. The frequency is displayed in units of twice the Fermi energy.

$\zeta_1,\ldots,\zeta_5$ are given in Table I in a proper order. The numerical evaluation of $I(q,\omega)$ using Eq. (67) can be implemented by means of either a multidimensional integration procedure or the Monte Carlo method. It should be noted that for $\omega>\omega_{1P+(q)}$ we have always $a_0>0$, so $\theta(a_0)=1$, and therefore the whole volume of the hypercube contributes to $I(q,\omega)$. For $\omega<\omega_{1P-}(q)$ the value $\theta(a_0)=0$ may occur in some region of the (ζ_1,ζ_2) unit square, which, finally, covers the whole square when ω approaches the limit $\omega_{2P-}(q)$, in agreement with the result of Sec. II.

VII. DISCUSSION AND CONCLUSION

The energy-loss function $\mathrm{Im}[-1/\epsilon(q,\omega)]$ is now calculated for selected two-dimensional systems by taking the proper polarizability $\Pi(q,\omega)$ in the following approximation (for $\omega>0$):

$$\mathrm{Im}\Pi(q,\omega)\approx\begin{cases}\mathrm{Im}\Pi_0(q,\omega) & \text{for } \omega_{\min}^{1\mathrm{Pair}}(q)<\omega<\omega_{\max}^{1\mathrm{Pair}}(q)\\ \mathrm{Im}\Pi^{2\mathrm{Pair}}(q,\omega) & \text{for remaining } \omega\end{cases} \tag{68}$$

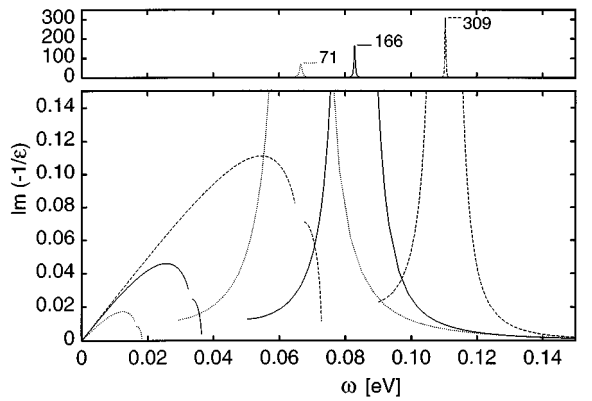

FIG. 3. The same as Fig. 2, but with the frequency displayed in units of eV.

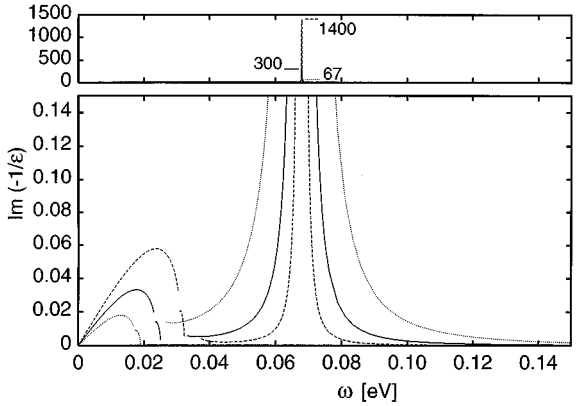

FIG. 4. Energy-loss function of an electron layer at $r_s=0.7$, calculated with the unscreened interaction. Dashed line: $N_d=1$, $q=0.046k_F$; full line: $N_d=2$, $q=0.070k_F$; dotted line: $N_d=4$, $q=0.104k_F$.

and

$$\mathrm{Re}\Pi(q,\omega)\approx\mathrm{Re}\Pi_0(q,\omega). \tag{69}$$

This is, in essence, a ''leading term'' approximation: the imaginary part of the Lindhard function is used in the frequency range of the single-pair excitation strip, while outside this range, the smallest-order nonzero (namely the second order) contribution due to two-pair excitations is used. There is no need to include the two-pair contribution within the single-pair strip, because there it would be a second-order correction only. Then the real part of the approximate $\Pi(q,\omega)$ can be obtained from $\mathrm{Im}\,\Pi(q,\omega)$ by means of the Hilbert transform. But the contribution due to the transformed $\mathrm{Im}\,\Pi^{2\mathrm{Pair}}$ from Eq. (68) can be neglected for all frequencies, as a second-order correction to the zeroth-order $\mathrm{Re}\,\Pi_0(q,\omega)$. Represented by a one-fermion-loop diagram, $\Pi_0(q,\omega)$ is proportional to N_d [cf. Eq. (20) for the second-order polarizability]. Thus the Lindhard function (known for paramagnetic electron liquid) multiplied by $(N_d/2)$ gives Π_0 for arbitrary N_d.[40]

In the following we discuss the resulting energy-loss function (ELF) with respect to its dependence on the degeneracy, momentum, and frequency, together with the influence of the model used for screening. For all presented results no lines are drawn in the vicinity of the frequencies $\omega_{1P\pm}$, where perturbation theory is not applicable.

In Figs. 2–4 $\mathrm{Im}\,[-1/\epsilon]$ is shown for three different degeneracies, $N_d=1$, 2, and 4. A starting point is the result for ELF displayed in Fig. 2 in the system units at $q=0.1$ (note the same upper bound of the single-pair excitations for all three curves). Both the dispersion and the broadening of the plasmon peak can be seen clearly. It should be mentioned that for small q the dispersion is given by $\omega_{\mathrm{pl}}(q)=\frac{1}{2}N_d^{3/4}(r_sq)^{1/2}$. Figure 3 then shows the same three curves, plotted with the energy transfer measured in eV (for recalculation the effective mass and the background dielectric constant corresponding to a Si-SiO_2 MOSFET have been used). A ''reversed'' ordering of the plasmon peaks positions is observed. The dependence of the plasmon's width on N_d is less pronounced in comparison to the previous figure, but still clearly to be seen. Finally, in Fig. 4, we compare plas-

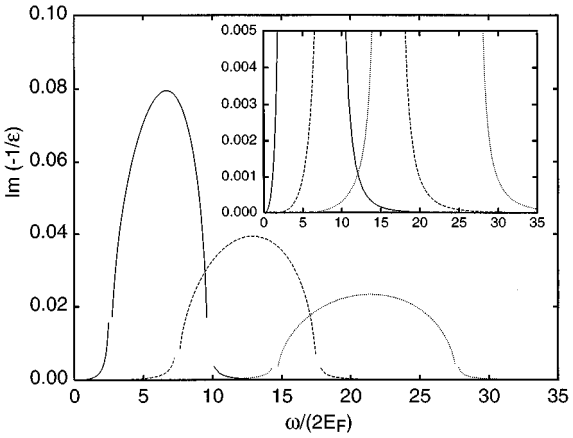

FIG. 5. Energy-loss function of an electron layer at $r_s=0.7$, calculated with the unscreened interaction. The curves correspond to the momenta $q=3.5k_F$ (full line), $q=5.0k_F$ (dashed line), and $q=6.5k_F$ (dotted line). Inset: the same plot with a magnified ordinate.

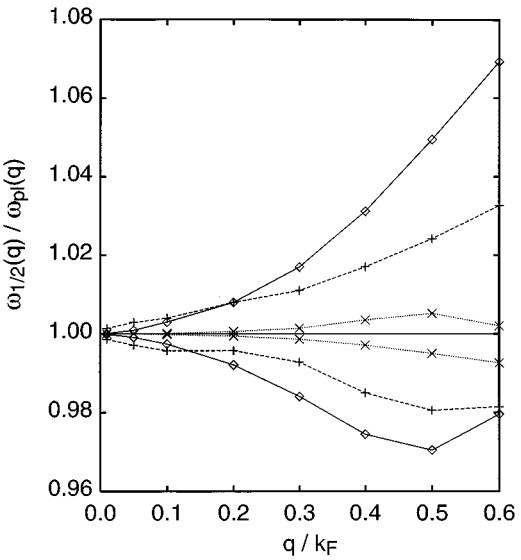

FIG. 6. Relative width of the plasmon peak of an electron layer at $r_s=0.7$, calculated with variously screened interactions. The upper and lower lines representing the frequencies at half height are shown with the same line type. Full lines: unscreened result; dotted lines: overall-screened result; dashed lines: selectively screened result.

mons measured at a particular energy, but arising in the three systems of the same electron density and different degeneracies. This can be obtained only by choosing different momentum transfers (in the effective atomic units, $qa_B^*=0.13$, 0.14, and 0.15 for $N_d=1$, 2, and 4, respectively). While these momenta differ by only 7%, observed enormous differences in widths indicate their strong dependence on N_d. (We also note that the $N_d=4$ curves of Figs. 3 and 4 are almost the same.)

Figure 5 gives the energy-loss function in the large-q region, where plasmon excitations are impossible. However, results in this region may be of interest for interpreting stopping power experiments.[37] For each q the single-pair peak (the RPA result) is seen, surrounded on both sides by tails due to two-pair excitations. The low-frequency tail starts at the finite frequency ω_{2P-}, Eq. (17), whereas the high-frequency tail spreads to infinity, although it diminishes rapidly, as is clearly seen in the inset.

Finally, the influence of screening is displayed in Fig. 6. Because the peak around the plasma frequency, $\omega_{\rm pl}(q)$, is not symmetric, two frequencies at half height, $\omega_{1/2}(q)$, situated on both sides of the peak, are shown. The tendency for the asymmetry is seen to grow with q. For small q the width of plasmons due to the selectively screened interaction exceeds the bare interaction result, yielding a nonvanishing value in the $q\to 0$ limit, while the width due to the overall screened interaction is seen to be the smallest one. Thus Fig. 6 shows that the width of a plasmon peak is extremely sensitive to the screening type applied in the evaluation of $\mathrm{Im}\,\Pi^{\rm 2Pair}$.

In order to gain some general understanding of this fact, we calculated $\mathrm{Im}\,\epsilon^{\rm 2Pair}(q,\omega)=-v(q)\mathrm{Im}\,\Pi^{\rm 2Pair}(q,\omega)$ for a series of r_s, with the remaining parameters kept fixed ($N_d=2$, $q=0.1k_F$, and $\omega=0.24\times 2E_F$ corresponding to the plasmon peak position at $r_s=0.7$). It should be recalled here that the plasmon width is, roughly speaking, proportional to $\mathrm{Im}\,\epsilon$ at the peak frequency; see, e.g., Ref. 20. The values of $\epsilon''_{\rm tot}=\mathrm{Im}\,\epsilon^{\rm 2Pair}$, given in Table II, are separated there into contributions due to various diagrams for $\mathrm{Im}\,\Pi^{\rm 2Pair}$,

$$\epsilon''_{\rm tot}=\epsilon''_{[2b]}+\epsilon''_{[2a]}+\epsilon''_{[1a]}, \tag{70}$$

TABLE II. Values of $\epsilon''=\mathrm{Im}\,\epsilon^{\rm 2Pair}(q=0.1k_F,\ \omega=0.24\times 2E_F)$ and of the contributions to it due to the different types of diagrams.

	Selective screening				Overall screening			
r_s	$\frac{100e''_{\rm tot}}{r_s^3}$	$\frac{\epsilon''_{[2b]}}{\epsilon''_{\rm tot}}$	$\frac{\epsilon''_{[2a]}}{\epsilon''_{\rm tot}}$	$\frac{\epsilon''_{[1a]}}{\epsilon''_{\rm tot}}$	$\frac{100\epsilon''_{\rm tot}}{r_s^3}$	$\frac{\epsilon''_{[2b]}}{\epsilon''_{\rm tot}}$	$\frac{\epsilon''_{[2a]}}{\epsilon''_{\rm tot}}$	$\frac{\epsilon''_{[1a]}}{\epsilon''_{\rm tot}}$
0^+	1.72	7.98	−6.72	−0.26	1.719	8.0	−6.7	−0.3
0.1	2.56	4.17	−3.05	−0.12	0.602	14.5	−13.0	−0.5
0.2	2.86	3.20	−2.12	−0.08	0.361	18.4	−16.8	−0.6
0.5	2.99	2.24	−1.20	−0.04	0.156	24.6	−22.8	−0.8
0.7	2.91	1.98	−0.95	−0.03	0.109	27.1	−25.3	−0.8
1.0	2.72	1.74	−0.72	−0.02	0.071	29.3	−27.4	−0.9
2.0	2.19	1.41	−0.40	−0.01	0.028	33.0	−31.1	−0.9
4.0	1.48	1.23	−0.22	−0.01	0.010	35.2	−33.3	−0.9

where the subscript $[2b]$ denotes the contribution due to sum of the two-fermion-loop diagrams [23], [24], and [25] (depending on the squared potential), the subscript $[2a]$ that due to the sum of the two-fermion-loop diagrams [21] and [22] (depending on the product of two potentials), and the subscript $[1a]$ that due to the sum of the one-fermion-loop diagrams [11], . . . ,[15] (depending on the product of the two potentials).

When q and ω are fixed, ϵ'' depends on r_s only via the potential factors and their screening. In particular, $v(k)$ is proportional to r_s when the system units are used. Thus three potential factors (two in the integrand of Π and one in the front of Π) provide the r_s^3 factor in ϵ'', which is accounted for in the way the results are presented in Table II. A remaining dependence on r_s stems from screening factors in the integrand. Therefore, the unscreened results, shown in the first row ($r_s \to 0$) of Table II, are valid, in fact, for all r_s. We see for them that the summary $\epsilon''_{\rm tot}$ value arises as an effect of a substantial cancellation between the positive $[2b]$ contribution, which is eight times larger than $\epsilon''_{\rm tot}$ itself, and the negative terms of remaining diagrams. Although the $[1a]$ contribution is much weaker than that of $[2b]$ or $[2a]$ taken separately, nevertheless its role is significant for the total result in almost all cases (except for the selective screening case in the $r_s > 0.5$ region). With increasing r_s (i.e., increasing strength of screening) the character of the observed cancellation changes: it is more and more pronounced in the case of overall screening, while it diminishes in the case of selective screening. This leads to drastically different plasmon peak widths at finite r_s: already at $r_s = 0.5$ the width corresponding to the selective screening is 20 times larger than that with overall screening, and at $r_s = 1$ it is 40 times larger; but, on the other hand, it is only 1.7, at least, times larger than the unscreened width.

This behavior may be explained by the form of the r_s dependence of the RPA static dielectric function used for screening. Let us recall that, in the system units, the Thomas-Fermi momentum is $k_{\rm TF} = 2^{1/2} r_s$, and $\epsilon^{\rm RPA}(k,0) \approx k_{\rm TF}/k$ for $k \ll k_{\rm TF}$, while $\epsilon^{\rm RPA}(k,0) \approx 1$ for $k \gg k_{\rm TF}$. Therefore, due to the factor $1/\epsilon^{\rm RPA}(k,0)$, the intergrands of selectively screened $[2b]$ diagrams gain an additional r_s^{-1} factor in such integration regions, where the argument k is small. For large enough r_s these regions cover almost the whole integration volume, and the diagrams become proportional to $r_s^3 r_s^{-1} = r_s^2$. The same reasoning applied to overall screened $[2b]$ diagrams and remaining screened diagrams (all having two such factors $1/\epsilon^{\rm RPA}$) leads to the dependence $r_s^3 r_s^{-2} = r_s^1$ for large r_s.

The results collected in Table III allow us to see how this predicted dependence develops in reality. The displayed logarithmic derivative of $\epsilon''_{\rm tot}$, $\epsilon''_{[2b]}$, etc. shows the effective exponent x in the representation of a particular function as proportional to r_s^x. We find that with increasing r_s these exponents diminish gradually from the value 3, characteristic for unscreened contributions, to the value 2.2 for the $[2b]$ selectively screened contribution and 1.4 for remaining diagram contributions (all at $r_s = 4$) showing a tendency to approach the predicted values 2 and 1 for very large r_s. Although, at moderate r_s, this difference in the exponents is less pronounced, nevertheless the different growth of SS and OS $\epsilon''_{[2b]}$ leads to weaker and stronger (respectively) cancellation effects, resulting in very different values of $\epsilon''_{\rm tot}$ for the two screenings discussed. Accordingly, the effective exponent of $\epsilon''_{\rm tot}$ is quite different than exponents of its separate contributions (except in the large-r_s region, where it is close to the exponent of the dominant contribution).

TABLE III. Logarithmic derivative $x = d \ln \epsilon''/d \ln r_s$ for the total ϵ'' and the separate contributions to it. Here $\epsilon'' = {\rm Im}\, \epsilon^{\rm 2Pair}(q = 0.1 k_F,\ \omega = 0.24 \times 2E_F)$.

	Selective screening				Overall screening			
r_s	$x_{\rm tot}$	$x_{[2b]}$	$x_{[2a]}$	$x_{[1a]}$	$x_{\rm tot}$	$x_{[2b]}$	$x_{[2a]}$	$x_{[1a]}$
0^+	3.0	3.0	3.0	3.0	3.0	3.0	3.0	3.0
0.1	3.1	2.8	2.7	2.6	2.3	2.7	2.7	2.6
0.2	3.1	2.7	2.6	2.5	2.3	2.5	2.6	2.5
0.5	2.9	2.6	2.3	2.3	2.0	2.2	2.3	2.3
0.7	2.8	2.5	2.1	2.1	1.9	2.1	2.1	2.1
1.0	2.8	2.4	2.1	2.0	1.8	1.9	2.1	2.0
2.0	2.5	2.3	1.7	1.6	1.5	1.7	1.7	1.6
4.0	2.3	2.2	1.4	1.4	1.4	1.4	1.4	1.4

The two different concepts of an effective (screened) interaction in the perturbational analysis of plasmon damping, investigated by us, can thus be summarized as follows. Both approaches seem to show a close resemblance and, in particular, are using principally the same formalism. Thus it is especially important to discuss the fundamental differences among them in more detail.

The first method, which we refer to within the present paper as *overall screening*, was in its basic concept developed by Glick and Long.[19] It tries to take into account higher-order effects in a global way by replacing *all* Coulomb potentials in the second-order expression for ${\rm Im}\, \Pi^{\rm 2Pair}$ by an effective interaction. Physically, this can be interpreted as an *a priori* introduction of the finite ''effective range of electron-electron interaction already within the electron gas Hamiltonian. Such an anticipation of the shielding effects in the many-electron collective has the main disadvantage that it makes the theory more distant from the first principles. However, calculations using this method have been successfully compared with experiments as well as other theoretical approaches,[35] so it nevertheless appears that they correctly represent relevant aspects of the problem.

On the other hand, starting from the fundamental perturbation series for the proper polarizability, it is shown in Sec. V that not all interaction lines in various second-order diagrams are equally replaced by an effective potential, when systematically taking into account higher-order effects. This method is denoted by *selective screening* within the present work. Although it has the obvious advantage of following the pure first principles more closely, it also raises nontrivial problems, as is shown by our numerical analysis: it appears that the approach of selective screening more easily breaks down, i.e., leads to unphysical results, when going to moderately low densities or small wave vectors. For example, the fact that, for $q \to 0$, the plasmon half-width remains finite demonstrates that even rather fundamental large-scale symmetry properties of the system can be sensitive to an inconsistent choice of the effective interaction: it is most probable

that this particular problem will be solved by using an appropriate dynamic screening function.

Closing the above discussion, the two ways of introducing shielding effects into a model based on finite-order perturbation theory should be considered as two different approximations, rather than two aspects of a single approach. Consequently, the two methods have their advantages and disadvantages: using overall screening leads to results with no obvious breakdown of the model; the more fundamental approach of selective screening, however, provides the basis for a systematic, completely first-principles-based analysis.

In summary, in this paper we present an analytical and numerical analysis of the imaginary part of the proper polarizabilty Eq. (4) for electron systems. Since both the space dimensionality and the electron band degeneracy enter our calculations as arbitrary parameters, a wide applicability to many systems is possible. Within the framework of a perturbational expansion, a low-frequency cutoff Eq. (17), characteristic of each n-pair process, is derived as an exact property. Concentrating on the leading terms, i.e., the two-pair processes, numerical results concerning the energy-loss function are presented for an electron layer with various band degeneracy factors, which represents an important model system for two-dimensional semiconductor devices. Going beyond the bare perturbational evaluation, the effects of screening on a plasmon peak width are studied. It appears to be of great importance to distinguish clearly between the two conceptionally different methods of building effective interactions into the theory, as is discussed in detail earlier in this section. Although a more extensive comparison of various screening ansatzes must be left to future work, it is quite likely that the fundamental approach proposed in this paper will provide an important tool to unify them finally into a promising theoretical description.

ACKNOWLEDGMENTS

One of us (M.E.B.) wants to express her deep gratitude to the late Professor W. Macke, who was her advisor for the doctoral thesis on which this contribution is based, and she thanks Professor U. M. Titulaer for helpful discussions. This work was partially carried out during our participation in the Workshop on Condensed Matter Physics at the International Center for Theoretical Physics, Trieste, Italy. Our thanks are due to the I.C.T.P. for its hospitality, and to Professor M. Tosi for his interest in this work. We also acknowledge financial support by the ''Rat für Auslandsbeziehungen der Johannes Kepler Universität.'' Part of the work was supported by the Austrian ''Fonds zur Förderung der wissenschaftlichen Forschung,'' Project No. P09504-PHY.

APPENDIX A: DERIVATION OF THE LOWER BOUND $\omega_{\min}^{n\mathrm{Pair}}(q)$

In determining $\omega_{\min}^{n\mathrm{Pair}}(q)$, first the minimization is considered in a subspace of $\boldsymbol{\alpha}$ where its all components α_j are positive ($j=1,\ldots,n$). The result of this minimization will be denoted by ${}^{+}\omega_{\min}^{n\mathrm{Pair}}(q)$. When substituting $\omega_{\min}^{1\mathrm{Pair}}(k)$ into the right-hand side of Eq. (10) we first use $\omega_{1P-}(k)$ in the whole range rather than the full expression given in Eq. (13). This procedure is correct, provided that the resulting solution $\boldsymbol{\alpha}^0$ is checked to lie in the region $\alpha_j^0 q > 2k_F$ for each j. So Eq. (10) is rewritten as

$$ {}^{+}\omega_{\min}^{n\mathrm{Pair}}(q) = \min\left\{ \frac{1}{2}\, q^2 \left(\sum_{j=1}^{n} \alpha_j^2 \right) - k_F q \left(\sum_{j=1}^{n} \alpha_j \right) \right\}. \tag{A1} $$

Because of the constraint (9), the term linear in q does not depend on $\boldsymbol{\alpha}$. The coefficient at $q^2/2$ is just the squared radius vector $\boldsymbol{\alpha}$, the end of which lies on the hyperplane $\alpha_1+\cdots+\alpha_n=1$. The shortest $\boldsymbol{\alpha}$ is perpendicular to this plane, so the solution is

$$ \boldsymbol{\alpha}^0 = \left(\frac{1}{n}, \ldots, \frac{1}{n} \right). \tag{A2} $$

Substituting $\boldsymbol{\alpha}=\boldsymbol{\alpha}^0$ into Eq. (A1) gives

$$ {}^{+}\omega_{\min}^{n\mathrm{Pair}}(q) = \omega_{nP-}(k)\,\theta(\omega_{nP-}(k)), \tag{A3} $$

with $\omega_{nP-}(k)$ defined in Eq. (18). This result can be used for $\alpha_j^0 q = (1/n)q > 2k_F$, as mentioned above. The zero result for $q < 2nk_F$, included already in Eq. (A3), can be obtained by inserting $\boldsymbol{\alpha}^0$ as a trial $\boldsymbol{\alpha}$ in Eq. (10), and then using result (13) to get 0. Since $\omega_0 \geqslant 0$ is of interest, other trial $\boldsymbol{\alpha}$ cannot ''improve'' the zero lower bound for it.

Now we allow some α_j to be negative during the minimization in Eq. (10). Let the number of positive α_j be n^+, and the number of negative α_j be $n^- = n - n^+$. In terms of two sets $\{\alpha_l^+ > 0, l=1,\ldots,n^+ : \alpha_1^+ + \cdots + \alpha_{n^+}^+ = 1\}$ and $\{\alpha_l^- > 0, l=1,\ldots,n^- : \alpha_1^- + \cdots + \alpha_{n^-}^- = 1\}$ and a parameter $x \geqslant 0$, we define α_j, satisfying the constraint $\alpha_1+\cdots+\alpha_n=1$, to be

$$ \alpha_j = \begin{cases} (1+x)\alpha_j^+ & \text{for } j=1,\ldots,n^+ \\ -x\alpha_{j-n^+}^- & \text{for } j=n^++1,\ldots,n. \end{cases} \tag{A4} $$

So Eq. (10) can be rewritten as

$$ \omega_{\min}^{n\mathrm{Pair}}(q) = \min_{1 \leqslant n^+ \leqslant n} \min_{x \geqslant 0} \left\{ \left[\min_{\substack{\alpha_1^+ > 0, \ldots, \alpha_{n^+}^+ > 0 \\ \alpha_1^+ + \cdots + \alpha_{n^+}^+ = 1}} \sum_{j=1}^{n^+} \omega_{\min}^{1\mathrm{Pair}}[\alpha_j^+ (1+x) q] \right] + \left[\min_{\substack{\alpha_1^- > 0, \ldots, \alpha_{n^-}^- > 0 \\ \alpha_1^- + \cdots + \alpha_{n^-}^- = 1 \\ n^- = n - n^+}} \sum_{j=1}^{n^-} \omega_{\min}^{1\mathrm{Pair}}(\alpha_j^- x q) \right] \right\}. \tag{A5} $$

By applying result (A3) of the minimization in the positive α_j subspace to each square bracket, we get

$$\omega_{\min}^{n\text{Pair}}(q)=\min_{1\leqslant n^+\leqslant n}\min_{x\geqslant 0}\{{}^+\omega_{\min}^{(n^+)\text{Pair}}[(1+x)q] + {}^+\omega_{\min}^{(n-n^+)\text{Pair}}(xq)\}. \tag{A6}$$

Since ${}^+\omega_{\min}^{l\text{Pair}}(k)$ is a nondecreasing function of k, the minimum (A6) is reached at $x=0$:

$$\omega_{\min}^{n\text{Pair}}(q)=\min_{1\leqslant n^+\leqslant n}{}^+\omega_{\min}^{(n^+)\text{Pair}}(q). \tag{A7}$$

Finally, since ${}^+\omega_{\min}^{l\text{Pair}}(q)$ is a nonincreasing function of l, the minimum in Eq. (A7) is obtained for $n^+=n$. So we demonstrated that

$$\omega_{\min}^{n\text{Pair}}(q)={}^+\omega_{\min}^{n\text{Pair}}(q), \tag{A8}$$

which is given in Eq. (17) in the main text.

APPENDIX B: EVALUATION OF DIAGRAMS

The contribution to the proper polarizability $\text{Im}\,\Pi(q,\omega)$ due to one of the diagrams shown on Fig. 1, say diagram a, can be written as[38,41]

$$\Omega_D^3\Pi_{[a]}(\mathbf{q},q_0)=-(-N_d)^{N_{\text{fl}}}\sum_{\mathbf{l},\mathbf{m},\mathbf{p}}\hat{V}_{[a]}\hat{G}_{[a]}, \tag{B1}$$

where N_{fl} is the number of fermion loops in a and N_d the total degeneracy of the electron band, see Eq. (3). The summation goes over three intermediate momenta $\mathbf{l}$, $\mathbf{m}$, and $\mathbf{p}$, and the remaining factors represent the two interactions in the diagrams (dashed lines), which are supposed to be static (frequency independent)

$$\hat{V}_{[a]}=v(\ldots)v(\ldots), \tag{B2}$$

and six Green functions (continuous lines), which are integrated out over all intermediate frequencies

$$\hat{G}_{[a]}=\int\frac{dl_0dm_0dp_0}{(2\pi i)^3}G(l+q)\ldots G(l). \tag{B3}$$

As an example, we evaluate now diagrams 12 and 24 labeled as in Fig. 7. The $(D+1)$-dimensional vectors like $q=(\mathbf{q},q_0)$ and $l=(\mathbf{l},l_0)$ are indicated there. We see that $N_{\text{fl}}=1$ for diagram 12 and $N_{\text{fl}}=2$ for 24, and that their interaction factors are also different:

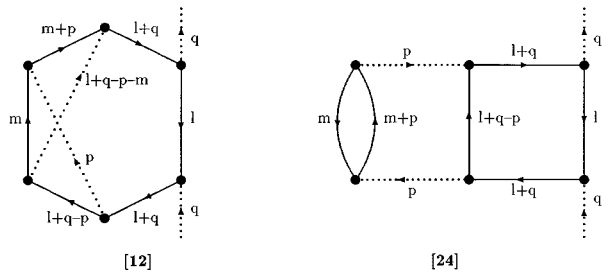

FIG. 7. Two of the diagrams of Fig. 1 shown with detailed information on internal 4-momenta.

$$\hat{V}_{[12]}=v(\mathbf{p})v(\mathbf{l}+\mathbf{q}-\mathbf{p}-\mathbf{m}), \tag{B4}$$

$$\hat{V}_{[24]}=[v(\mathbf{p})]^2, \tag{B5}$$

while the Green-function factors are common:

$$\hat{G}_{[12]}=\hat{G}_{[24]}=\int\frac{dl_0dm_0dp_0}{(2\pi i)^3}G(l+q)\times G(l+q-p)G(m)G(m+p)G(l+q)G(l). \tag{B6}$$

Actually, all remaining diagrams may be arranged in pairs and labeled in such a way that $\hat{G}_{[11]}=\hat{G}_{[23]}$, $\hat{G}_{[13]}=\hat{G}_{[25]}$, $\hat{G}_{[14]}=\hat{G}_{[21]}$, and $\hat{G}_{[15]}=\hat{G}_{[22]}$, while their interaction factors are different. The Green function used in Eqs. (B3) and (B6) is

$$G(k)\equiv G(\mathbf{k},k_0)=n_{\mathbf{k}}^-[k_0-(\epsilon_{\mathbf{k}}-i\eta)]^{-1}+n_{\mathbf{k}}^+[k_0-(\epsilon_{\mathbf{k}}+i\eta)]^{-1},\quad \eta\to 0^+ \tag{B7}$$

[see Eqs. (7) and (22) for the definitions of $n_{\mathbf{k}}^{\pm}$ and ϵ_k]. This $G(k)$ leads to the time-ordered version of $\Pi_{[a]}(\mathbf{q},q_0)$ when $\hat{G}_{[a]}$ obtained in Eq. (B6) is inserted into Eq. (B1). The retarded version, used in the electron response applications, can be readily obtained from the above version by shifting its poles, i.e., by replacing $(q_0\pm i\eta)$ with $(q_0+i\eta)$ in each denominator of the result of the integrations in Eq. (B3). So we obtain

$$\begin{aligned}\hat{G}_{[12]}=\hat{G}_{[24]}=&[n_{\mathbf{m}+\mathbf{p}}^+n_{\mathbf{l}+\mathbf{p}}^+n_{\mathbf{l}+\mathbf{q}-\mathbf{p}}^+n_{\mathbf{m}}^-n_{\mathbf{l}}^- -\text{o.o.}][q_0+i\eta-(\epsilon_{\mathbf{m}+\mathbf{p}}+\epsilon_{\mathbf{l}+\mathbf{q}-\mathbf{p}}-\epsilon_{\mathbf{m}}-\epsilon_{\mathbf{l}})]^{-1}[q_0+i\eta-(\epsilon_{\mathbf{l}+\mathbf{q}}-\epsilon_{\mathbf{l}})]^{-2}\\&-[n_{\mathbf{m}}^+n_{\mathbf{l}}^+n_{\mathbf{l}+\mathbf{q}}^+n_{\mathbf{m}+\mathbf{p}}^-n_{\mathbf{l}+\mathbf{q}-\mathbf{p}}^- -\text{o.o.}][q_0+i\eta-(\epsilon_{\mathbf{m}+\mathbf{p}}+\epsilon_{\mathbf{l}+\mathbf{q}-\mathbf{p}}-\epsilon_{\mathbf{m}}-\epsilon_{\mathbf{l}})]^{-1}[\epsilon_{\mathbf{m}+\mathbf{p}}+\epsilon_{\mathbf{l}+\mathbf{q}-\mathbf{p}}-\epsilon_{\mathbf{m}}-\epsilon_{\mathbf{l}+\mathbf{q}}]^{-2}\\&+[n_{\mathbf{m}+\mathbf{p}}^+n_{\mathbf{l}}^+n_{\mathbf{l}+\mathbf{q}-\mathbf{p}}^+n_{\mathbf{m}}^-n_{\mathbf{l}+\mathbf{q}}^- -\text{o.o.}]\{[q_0+i\eta-(\epsilon_{\mathbf{l}+\mathbf{q}}-\epsilon_{\mathbf{l}})]^{-2}[\epsilon_{\mathbf{m}+\mathbf{p}}+\epsilon_{\mathbf{l}+\mathbf{q}-\mathbf{p}}-\epsilon_{\mathbf{m}}-\epsilon_{\mathbf{l}+\mathbf{q}}]^{-1}\\&+[q_0+i\eta-(\epsilon_{\mathbf{l}+\mathbf{q}}-\epsilon_{\mathbf{l}})]^{-1}[\epsilon_{\mathbf{m}+\mathbf{p}}+\epsilon_{\mathbf{l}+\mathbf{q}-\mathbf{p}}-\epsilon_{\mathbf{m}}-\epsilon_{\mathbf{l}+\mathbf{q}}]^{-2}\}.\end{aligned} \tag{B8}$$

Here o.o. means the opposite occupation term, i.e., obtained from the preceding term by applying the replacement $n_{\mathbf{k}}^{\pm}\to n_{\mathbf{k}}^{\mp}$ in each occupation factor. We see the poles at the two-particle-hole pair excitation energy in the first and second terms of the right-hand side of Eq. (B8). Therefore $\text{Im}\,\Pi_{[a]}^{2\text{Pair}}$ can be calculated according to Eq. (B1) for $q_0=\omega$ using the following two terms of $\text{Im}\,\hat{G}_{[a]}$:

$$\mathrm{Im}\,\hat{G}^{2\mathrm{Pair}}_{[12]}=\mathrm{Im}\,\hat{G}^{2\mathrm{Pair}}_{[24]}=-n^{-}_{\mathbf{m}+\mathbf{p}}n^{-}_{\mathbf{l}+\mathbf{q}}n^{-}_{\mathbf{l}+\mathbf{q}-\mathbf{p}}n^{+}_{\mathbf{m}}n^{+}_{\mathbf{l}}(-\pi)\,\delta[\omega-(\epsilon_{\mathbf{m}+\mathbf{p}}+\epsilon_{\mathbf{l}+\mathbf{q}-\mathbf{p}}-\epsilon_{\mathbf{m}}-\epsilon_{\mathbf{l}})]\{(\epsilon_{\mathbf{m}+\mathbf{p}}+\epsilon_{\mathbf{l}+\mathbf{q}-\mathbf{p}}-\epsilon_{\mathbf{m}}-\epsilon_{\mathbf{l}+\mathbf{q}})^{-2}\}_{\mathrm{Re}}$$
$$-n^{-}_{\mathbf{m}+\mathbf{p}}n^{-}_{\mathbf{l}+\mathbf{q}-\mathbf{p}}n^{+}_{\mathbf{l}+\mathbf{q}}n^{+}_{\mathbf{m}}n^{+}_{\mathbf{l}}(-\pi)\,\delta[\omega-(\epsilon_{\mathbf{m}+\mathbf{p}}+\epsilon_{\mathbf{l}+\mathbf{q}-\mathbf{p}}-\epsilon_{\mathbf{m}}-\epsilon_{\mathbf{l}})](\epsilon_{\mathbf{m}+\mathbf{p}}+\epsilon_{\mathbf{l}+\mathbf{q}-\mathbf{p}}-\epsilon_{\mathbf{m}}-\epsilon_{\mathbf{l}+\mathbf{q}})^{-2} \quad \text{(B9)}$$

[the terms due to the positive excitation energy only should be included; see Eq. (19)]. We introduced the symbol $\{f\}_{\mathrm{Re}}$ defined for f in terms of natural $n_1,n_2,\ldots$ and real $x,y\ldots$,

$$\{x^{-n_1}y^{-n_2}\cdots\}_{\mathrm{Re}}=\lim_{0<\eta\to 0}\mathrm{Re}\{(x+i\eta)^{-n_1}(y+i\eta)^{-n_2}\cdots\}. \quad \text{(B10)}$$

This is a combination of principal-value and Dirac-delta distributions and their derivatives, with arguments $x,y,\ldots$. In the final step, in order to have the standard form shown in Eq. (19), we change the variables of summation into

$$\mathbf{q}_1=\mathbf{m},\quad \mathbf{q}_2=\mathbf{l},\quad \mathbf{q}_3=\mathbf{l}+\mathbf{q}-\mathbf{p},\quad \mathbf{q}_4=\mathbf{m}+\mathbf{p}. \quad \text{(B11)}$$

Then the contribution $\mathcal{F}_{[a]}$ of diagram a to $\mathrm{Im}\,\Pi^{2\mathrm{Pair}}$ corresponding to $\hat{V}_{[a]}\,\mathrm{Im}\,\hat{G}_{[a]}$ in Eq. (B1) can be written as

$$\mathcal{F}_{[a]}=\pi\hat{V}_{[a]}\hat{g}_{[a]}, \quad \text{(B12)}$$

where, for the considered diagrams, we have, from Eqs. (B4) and (B5),

$$\hat{V}_{[12]}=v_{41}v_{31}, \quad \text{(B13)}$$

$$\hat{V}_{[24]}=v^2_{41}, \quad \text{(B14)}$$

and from Eq. (B9)

$$\hat{g}_{[12]}=\hat{g}_{[24]}=-n^{-}_{2'}\{\omega^{-2}_{2'}\}_{\mathrm{Re}}-n^{+}_{2'}\omega^{-2}_{2'}. \quad \text{(B15)}$$

A compact form of Eq. (B15) and analogous results for the remaining diagrams are possible due to the shorthand notation for the occurring combinations of energies and momenta and for the potential, shown in Eqs. (25)–(27). All remaining diagrams can be evaluated in a similar way to give

$$\hat{V}_{[11]}=v_{41}v_{42}, \quad \text{(B16)}$$

$$\hat{V}_{[23]}=v^2_{41}, \quad \text{(B17)}$$

$$\hat{g}_{[11]}=\hat{g}_{[23]}=-n^{+}_{3'}\{\omega^{-2}_{3'}\}_{\mathrm{Re}}-n^{-}_{3'}\omega^{-2}_{3'}, \quad \text{(B18)}$$

$$\hat{V}_{[13]}=v_{31}v_{32}, \quad \text{(B19)}$$

$$\hat{V}_{[25]}=v^2_{31}, \quad \text{(B20)}$$

$$\hat{V}_{[14]}=v_{41}v_{31}, \quad \text{(B21)}$$

$$\hat{V}_{[21]}=v_{41}v_{32}, \quad \text{(B22)}$$

$$\hat{g}_{[13]}=\hat{g}_{[25]}=\hat{g}_{[14]}=\hat{g}_{[21]}=2n^{-}_{2'}n^{-}_{4'}\{\omega^{-1}_{2'}\}_{\mathrm{Re}}\omega^{-1}_{4'}$$
$$+2n^{+}_{2'}n^{+}_{4'}\omega^{-1}_{2'}\{\omega^{-1}_{4'}\}_{\mathrm{Re}}+2n^{-}_{2'}n^{+}_{4'}\{\omega^{-1}_{2'}\omega^{-1}_{4'}\}_{\mathrm{Re}}$$
$$+2n^{+}_{2'}n^{-}_{4'}\omega^{-1}_{2'}\omega^{-1}_{4'}. \quad \text{(B23)}$$

In diagrams 15 and 22 the energy ω_0 is found in two different representations in terms of **l**, **m**, and **p**; therefore Eq. (B12) must be replaced in this case by

$$\mathcal{F}_{[a]}=\pi\hat{V}^{A}_{[a]}\hat{g}^{A}_{[a]}+\pi\hat{V}^{B}_{[a]}\hat{g}^{B}_{[a]}, \quad \text{(B24)}$$

where

$$\hat{V}^{A}_{[15]}=v_{41}v_{31},\quad \hat{V}^{B}_{[15]}=v_{41}v_{42}, \quad \text{(B25)}$$

$$\hat{V}^{A}_{[22]}=\hat{V}^{B}_{[22]}=v_{41}v_{32}, \quad \text{(B26)}$$

$$\hat{g}^{A}_{[15]}=\hat{g}^{A}_{[22]}=-n^{-}_{3'}n^{-}_{4'}\omega^{-1}_{3'}\omega^{-1}_{4'}-n^{+}_{3'}n^{+}_{4'}\{\omega^{-1}_{3'}\omega^{-1}_{4'}\}_{\mathrm{Re}}$$
$$-n^{-}_{3'}n^{+}_{4'}\omega^{-1}_{3'}\{\omega^{-1}_{4'}\}_{\mathrm{Re}}-n^{+}_{3'}n^{-}_{4'}\{\omega^{-1}_{3'}\}_{\mathrm{Re}}\omega^{-1}_{4'}, \quad \text{(B27)}$$

$$\hat{g}^{B}_{[15]}=\hat{g}^{B}_{[22]}=-n^{-}_{1'}n^{-}_{2'}\{\omega^{-1}_{1'}\omega^{-1}_{2'}\}_{\mathrm{Re}}-n^{+}_{1'}n^{+}_{2'}\omega^{-1}_{1'}\omega^{-1}_{2'}$$
$$-n^{-}_{1'}n^{+}_{2'}\{\omega^{-1}_{1'}\}_{\mathrm{Re}}\omega^{-1}_{2'}-n^{+}_{1'}n^{-}_{2'}\omega^{-1}_{1'}\{\omega^{-1}_{2'}\}_{\mathrm{Re}}. \quad \text{(B28)}$$

After substituting the expressions for $\mathcal{F}_{[a]}$, given in Eqs. (B12)–(B28), into Eq. (19), $\mathrm{Im}\,\Pi^{2\mathrm{Pair}}$ can be obtained for arbitrary (q,ω) by means of $(3D-1)$-fold numerical integration (after taking into account the δ functions). However, because of the principal value and other distributions, generated by the symbol $\{f\}_{\mathrm{Re}}$ [see Eq. (B10)], this integration may be extremely difficult to perform in practice. But, if we assume that during integration all denominators satisfy $\omega_{i'}\neq 0$, the symbols $\{f\}_{\mathrm{Re}}$ reduce just to f. The region of the (q,ω) plane, where this assumption is satisfied, is determined in Sec. IV, while below the consequences of this assumption are taken into account.

The identity $n^{+}_{\mathbf{k}}+n^{-}_{\mathbf{k}}=1$ allows us to simplify the expressions for $\hat{g}_{[a]}$ when the symbol $\{\}_{\mathrm{Re}}$ is omitted, e.g., $\hat{g}_{[12]}=-\omega^{-2}_{2'}$ in Eq. (B15). The final result, obtained in analogous way, is given in Eqs. (23) and (24) of the main text.

[1] P. Schattschneider and B. Jouffrey, in *Energy-Filtering Transmission Electron Microscopy*, edited by L. Reimers, Springer Series in Optical Sciences Vol. 71 (Springer, New York, 1995), p. 151.
[2] P. Schattschneider, D. S. Su, and P. Pongratz, Scanning Microsc. **6**, 123 (1992).
[3] J. Sprösser-Prou, A. vom Felde, and J. Fink, Phys. Rev. B **40**, 5799 (1989).
[4] A. vom Felde, J. Sprösser-Prou, and J. Fink, Phys. Rev. B **40**, 10 181 (1989).
[5] W. Schülke, H. Nagasawa, S. Mourikis, and A. Kaprolat, Phys. Rev. B **40**, 12 215 (1989).
[6] P. M. Platzman, E. D. Isaacs, and H. Williams, Phys. Rev. B **46**, 12 943 (1992).
[7] W. Schülke, H. Schulte-Schrepping, and J. R. Schmitz, Phys. Rev. B **47**, 12 426 (1993).
[8] K. Sturm and L. Oliveira, Phys. Rev. B **24**, 3054 (1981).
[9] W. Schülke, H. Nagasawa, S. Mourikis, and F. Lanzki, Phys. Rev. B **33**, 6744 (1986).
[10] K. Awa, H. Yasuhara, and T. Asaki, Phys. Rev. B **25**, 3670 (1982); **25**, 3687 (1982).
[11] P. K. Aravind, A. Holas, and K. S. Singwi, Phys. Rev. B **25**, 561 (1982).
[12] J. Hong and M. H. Lee, Phys. Rev. Lett. **55**, 2375 (1985).
[13] F. Green, D. Neilson, and J. Szymanski, Phys. Rev. B **35**, 124 (1987); **35**, 133 (1987).
[14] F. Green, D. Neilson, and J. Szymanski, Phys. Rev. B **31**, 5837 (1985).
[15] A. Nakano and S. Ichimaru, Phys. Rev. B **39**, 4930 (1989); **39**, 4938 (1989).
[16] M. Rösler, W. Brauer, J. Devooght, J. C. Dehaes, A. Dubus, M. Cailler, and J. B. Ganachaud, *Particle Induced Electron Emission I*, Springer Tracts in Modern Physics Vol. 122 (Springer, New York, 1991).
[17] D. Hasselkamp, H. Rothard, K. O. Groeneveld, J. Kemmler, P. Varga, and H. Winter, *Particle Induced Electron Emission II*, Springer Tracts in Modern Physics Vol. 123 (Springer, New York, 1991).
[18] H. M. Böhm, S. Conti, and M. P. Tosi, J. Phys. Condens. Matter **8**, 781 (1996).
[19] A. Glick and W. Long, Phys. Rev. B **4**, 3455 (1971).
[20] A. Holas and K. S. Singwi, Phys. Rev. B **40**, 158 (1989).
[21] W. Gasser, Z. Phys. B **57**, 15 (1984).
[22] M. E. Bachlechner, H. M. Miesenböck, and W. Macke, Physica B **150**, 337 (1988).
[23] M. E. Bachlechner, W. Macke, H. M. Miesenböck, and A. Schinner, Physica B **168**, 104 (1991).
[24] W. Gasser, Physica B **183**, 217 (1992).
[25] T. Ando, A. B. Fowler, and F. Stern, Rev. Mod. Phys. **54**, 437 (1982).
[26] C. Weisbuch and B. Vinter, *Quantum Semiconductor Structures* (Academic, New York, 1991).
[27] G. Bastard, *Wave Mechanics Applied to Semiconductor Heterostructures* (Les Éditions de Physique, Les Ulis Cedex, 1992).
[28] R. A. Höpfel and E. Gornik, Surf. Sci. **142**, 412 (1984).
[29] N. T. Theis, J. P. Kotthaus, and P. J. Stiles, Solid State Commun. **26**, 603 (1978).
[30] S. J. Allen, D. C. Tsui, and R. A. Logan, Phys. Rev. Lett. **38**, 980 (1977).
[31] M. E. Bachlechner, *Two-Pair Effects in Simple Metals and Semiconductor Structures*, Schriften der Johannes Kepler Universität Linz, Reihe C, Band 9 (Universitätsverlag Rudolf Trauner, Linz, 1995).
[32] M. E. Bachlechner, H. M. Böhm, and A. Schinner, Phys. Lett. A **178**, 186 (1993).
[33] A. Isihara, in *Solid State Physics*, edited by H. Ehrenreich and O. Turnbull (Academic, New York, 1989), Vol. 42, p. 271.
[34] A. Isihara, Phys. Scr. **32**, 26 (1985).
[35] M. E. Bachlechner, H. M. Böhm, and A. Schinner, Physica B **183**, 293 (1993).
[36] A. Holas, P. K. Aravind, and K. S. Singwi, Phys. Rev. B **20**, 4912 (1979).
[37] A. Schinner, M. E. Bachlechner, and H. M. Böhm, Nucl. Instrum. Methods Phys. Res. Sect. B **93**, 181 (1994).
[38] R. D. Mattuck, *A Guide to Feynman Diagrams in the Many-Body Problem* (McGraw-Hill, London, 1967).
[39] K. Utsumi and S. Ichimaru, Phys. Rev. B **23**, 3291 (1981).
[40] M. Jonson, J. Phys. C **9**, 3055 (1976).
[41] A. Fetter and J. D. Walecka, *Quantum Theory of Many Particle Systems* (McGraw-Hill, New York, 1971).